Article

Properties of APTES-Modified CNC Films

Sadat Kamal Amit, Diego Gomez-Maldonado, Tiana Bish, Maria S. Peresin, and Virginia A. Davis*

Read Online

ACCESS | Metrics & More | Article Recommendations | Supporting Information

ABSTRACT: Sulfated cellulose nanocrystals' (CNCs') facile aqueous dispersibility enables producing films, fibers, and other materials using only water as a solvent but prevents using sulfated CNCs in applications that require water immersion. We report that modifying CNCs with 3-aminopropyl-triethoxysilane (APTES) via a simple, single-pot reaction scheme dramatically improves the hydrolytic stability of CNC films. The effects of APTES modification on CNCs' properties were studied using attenuated total reflectance Fourier transform infrared spectroscopy, atomic force and optical microscopy, thermogravimetric analysis, dynamic light scattering, and ultimate analysis. Substituting a mere 12.6% of the CNCs' available hydroxyl groups with APTES dramatically increased the hydrolytic stability of shear cast films while only having minor impacts on their mechanical properties. In addition, quartz crystal microbalance with dissipation monitoring (QCMD) and multiparametric surface plasmon resonance (MP-SPR) studies showed that the CNC-APTES films also had a greater irreversible binding with carbofuran, a pesticide and emerging contaminant. These results highlight that APTES modification is a promising method for increasing the utility of sulfated CNCs in sensors, adsorbents, and other applications requiring water immersion.
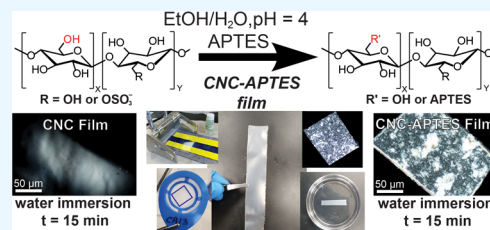
1. INTRODUCTION

Cellulose nanocrystals (CNCs) are exciting, naturally abundant one-dimensional anisotropic nanomaterials[1,2] that can be used in numerous commodity and advanced material applications, including those in the paper,[3] catalysis,[4] pharmaceutical,[5] and polymer[6] industries. While CNCs can be produced by bacteria, they are more commonly extracted from biomass resources such as wood, cotton, and soybean hulls.[7,8] CNCs are generally known for their high specific surface area and high specific strength; their exact properties depend on both the biomass source and extraction methodology. To date, much CNC research has focused on CNCs extracted from wood via sulfuric acid hydrolysis because these sulfated CNCs are commercially available and are easily dispersed in water.

CNCs' native hydroxyl groups make them inherently hydrophilic. The use of sulfuric acid to extract CNCs from biomass results in the partial substitution of these hydroxyl groups with sulfate half-ester groups. The resulting electrostatic repulsion makes sulfated CNC readily dispersible in water. This enables the use of aqueous processing to produce CNC films but also makes the resulting films inherently unstable in water. Significant research has been directed toward modifying CNCs' surface chemistry to enhance their suitability for different applications. For example, researchers have reported CNC modification using polymers such as polylactic acid,[9] polyphenols,[10] and chitosan,[11] surfactants such as cetyltrimethylammonium bromide (CTAB),[12] and several other compounds including isocyanates,[13] castor oil,[14] and butyric anhydride.[15] Many of these studies have been focused on increasing CNCs' hydrophobicity to facilitate their dispersion in polymers and organic solvents. Fewer researchers have focused on modifying CNCs with the intent of increasing the stability of CNC films in different solvents. Several works have focused on enhancing CNC film stability in solvents while retaining their chiral nematic ordering for photonic applications. For example, Hanif et al. utilized glutaraldehyde to create cross-linked films that were stable in a broad range of solvents, including water and toluene.[16] Zhang et al. used a combination of glutaraldehyde and poly(vinyl alcohol) to enhance both film stability and toughness.[17]

Silylation is a well-established functionalization method used to enhance hydrophobicity, thermal properties, and interfacial interactions with other materials. With regard to CNCs, researchers have used 3-isocyanatepropyltriethoxysilane (IPTS)-modified CNCs for reinforcing silicon rubber,[18] 3-mercaptopropyltrimethoxysilane (MPTMS, 95%)- and n-propyltriethoxysilane (PTS)-modified CNCs for froth floatation,[19] methyltrimethoxysilane-modified CNCs as a flame retardant material,[20] n-propyltriethoxysilane (PTS)- and 3-aminopropyl-triethoxysilane (APTES)-modified bifunctionalized CNCs for quartz microfloatation.[21] APTES is one of the most commonly used silylation agents due to its reactivity and ability to introduce amino functional groups for further functionalization reactions. For example, APTES-GA (gluta-
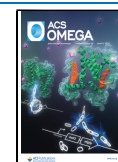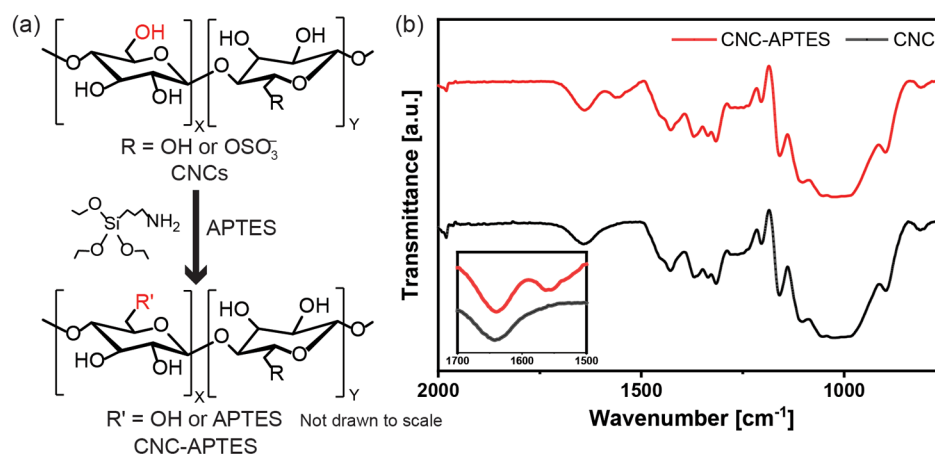
Figure 1. (a) Schematic representation of APTES functionalization of sulfated CNCs. (b) ATR-FTIR spectra of CNCs and CNC-APTES. The inset figure shows the presence of the additional N−H bending peak in CNC-APTES.

Table 1. Characterization Summary of CNC and CNC-APTES[a]

CNC type	N (%)	Si (%)	crystallinity index (%)	T_d (°C)	ζ-potential (mV)	charge density (μeq/gr)	conductivity (μS/cm)	hydrodynamic radius (nm)
CNC	0	0	67 (3)	240 (1.5)	−54 (1.22)	530 (90)	15.9 (0.22)	150 (2.0)
CNC- APTES	0.6 (0.01)	1.0 (0.03)	66 (1)	243 (2.0)	−34 (0.17)	180 (60)	7.3 (0.09)	770 (10)

[a]Numbers in the parentheses are standard error calculated based on a minimum of three runs. See Section 4 and Supporting Information for additional details.

raldehyde) chemistry is widely used to immobilize proteins and other biomolecules on nanomaterial surfaces.[22,23] A key challenge with APTES modification of nanomaterials is that APTES' ability to cross-link with itself can result in nanomaterial aggregation. This is typically mitigated by running reactions at relatively dilute concentrations. Other challenges are that prolonged reaction times can result in condensation of hydrolyzed APTES,[24] and the orientation of molecule on the surface can affect properties.[25]

In the case of sulfated CNCs, APTES reacts with surface hydroxyl groups, resulting in a surface-bound amino functionalized layer. Khanjanzadeh et al. established a scheme for producing silylated CNC hydrogels using 3-aminopropyltriethoxysilane (APTES, $C_9H_{23}NO_3Si$, ≥ 98%) and demonstrated that CNC-APTES had enhanced thermal stability compared to the initial sulfated CNC.[26] After this, several researchers utilized APTES-modified CNCs for uses such as immobilization supports for nanoparticles,[27] coating agents to alter interphase interactions,[28] and in nanocomposite membranes used for metal removal and dye adsorption.[29] Nori et al. used glutaric anhydride to link CNC-APTES that had been modified with antibodies used in cancer biomarker detection.[30] The resulting CNC-APTES-antibody films had sufficient hydrolytic stability to enable prolonged quartz crystal microbalance with dissipation (QCMD) monitoring using phosphate-buffered saline as the medium.[30] However, to the best of the authors' knowledge, the collective effects of APTES modification on CNC films' hydrolytic stability, mechanical properties, and ability to act as nonspecific sensors or adsorbents have not previously been studied. This work bridges these knowledge gaps by covalently attaching APTES to CNCs dispersed in water and quantifying the degree of functionalization along with changes in hydrolytic stability, mechanical properties, and binding of carbofuran.

2. RESULTS AND DISCUSSION

2.1. CNC-APTES Characterization. In this work, sulfated CNCs extracted from woody biomass (CelluForce NCC Dispersion NCV-100, Montreal, Canada) were modified according to the procedure for CNC dispersions reported by Nori et al.[30] A schematic of the APTES functionalization of the sulfated anhydroglucose unit is shown in Figure 1a. The initial and APTES-modified CNCs were characterized using attenuated total reflectance Fourier transform infrared spectroscopy (ATR-FTIR), ultimate analysis, inductively coupled plasma mass spectroscopy (ICP-MS), X-ray diffraction (XRD), and thermogravimetric analysis (TGA). The particle size, ζ-potential, charge, and conductivity were also measured (see the Materials and Methods and Supporting Information, Figures S1−S4)

The presence of APTES was qualitatively confirmed based on the presence of primary amine N−H bending (1650−1580 cm^{-1}) vibrations[26] in the ATR-FTIR spectra (Figure 1b). Additional characterization results are listed in Table 1. Quantifying the degree of substitution (DS) on CNCs is a known challenge due to the relatively low number of surface hydroxyl groups available for functionalization and the need to use multiple analytical methods, all of which have some experimental limitations.[31] In this study, the DS was calculated based on the number of hydroxyl groups available on the CNCs' surfaces, and the weight percent of nitrogen was determined using ultimate analysis.[32] The number of available hydroxyl groups on a CNC's surface was determined based on the model predicted by Eyley and Thielemans[31] using eq 1.

$$N_{OH} = \frac{n_1 + n_2}{\rho N_A L_1 L_2 c}\left(\frac{L_1 + L_2}{d_{(110)}} + \frac{L_1 + L_2}{d_{(1\bar{1}0)}}\right)$$
$$+ 2(\rho N_A L_3 d_{(110)} d_{(1\bar{1}0)})^{-1} \tag{1}$$
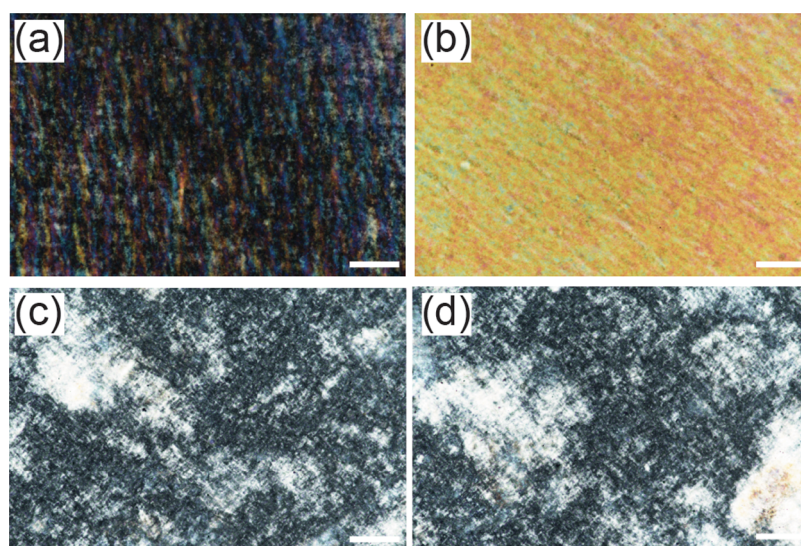
Figure 2. Polarized optical microscopy image of the shear cast CNC film showing alignment texture; analyzer (a) at 0°, (b) at 45° with flow direction; shear cast CNC-APTES film showing no significant texture due to alignment; analyzer (c) at 0°, (d) at 45° with the flow direction. Scale bar: 100 μm.

where L_1, L_2, and L_3 define the height, width, and length of the CNCs, respectively, $d_{(110)}$ and $d_{(1\bar{1}0)}$ are the horizontal and vertical unit cell dimensions of CNCs, respectively, n_1 and n_2 are the number of primary −OH groups facing (110) and $(1\bar{1}0)$ planes in the unit cell, respectively, ρ is the density, c is the unit cell dimension, and N_A stands for the Avogadro's number. The parameters used in the equation are given in Table S1. Based on this equation, the average number of available hydroxyl groups on a pristine CNC surface is 1.9 mmol/g, but some of these are converted to sulfate half-ester groups during the acid hydrolysis used for CNC extraction. Based on conductometric titration (Figure S3), the sulfate half-ester content was found to be 0.13 mmol/g (0.4 wt %). Ultimate analysis showed the nitrogen content was 0.6 wt %, and ICP-MS showed the amount of silicon was 1 wt %. The difference between the resulting 0.9:1.0 N/Si atomic ratio and the expected 1:1 ratio is attributed to experimental error. Based on these results, the degree of −OH substitution by APTES was DS = 12.6%. This degree of substitution did not significantly affect the crystallinity index, as measured by X-ray diffraction (XRD), or the thermal degradation temperature, as measured by thermal gravimetric analysis (TGA) (Figure S4). However, the substitution of −OH groups with APTES decreased the charge density and the conductivity of the CNC dispersion (Table 1). APTES modification also decreased the colloidal stability of CNCs in water. The ζ-potential increased from −54 to −34 mV. While −34 mV still indicates colloidal stability,[33] there was a marked change in the hydrodynamic radius measurements. The measured hydrodynamic radius is a function of the volume swept by the particle. For rod-like colloids, this generally relates to the largest dimension. For CNC, the average hydrodynamic radius was consistently around 150 nm, which is consistent with the 160 ± 36 nm average length measured by AFM. In addition, the hydrodynamic radius measurements had a log-normal size distribution (Figure S5), consistent with the expected CNC polydispersity. However, CNC-APTES had a much larger average hydrodynamic radii ranging between 420 and 770 nm between samples. Some particles even measured over 10 μm. This is largely attributed to end-to-end cross-linking of CNC

by APTES, although the AFM height images (Figure S6) also showed some side-to-side aggregation. Some aggregates were large enough to distort cross-polarized optical microscopy images. Previous work showed that CNC-APTES aggregates became larger and more numerous with increasing concentration,[34] which could result in less available surface area for further modification and nonuniform macroscale properties. The CNC and APTES concentrations used in this study were optimized by Nori, to achieve enough colloidal stability for further surface reactions.[34]

2.2. Impact of APTES Modification on Alignment of CNCs in Shear Cast Films. With increasing concentration, the aqueous CNC dispersions exhibited the expected lyotropic liquid crystalline phase behavior (Figure S7). For CNCs, a liquid crystalline dispersion concentration of 3.2 vol % (5.0 wt %) was chosen for film preparation to increase the amount of alignment in the final film.[35,36] However, the CNC-APTES dispersions did not exhibit liquid crystalline phase behavior at any concentration. Moreover, they appeared more viscous than an equivalent concentration of CNC; this limited the range of concentrations that could be cast into films. Based on processing constraints, a concentration of 1.8 vol % (2.8 wt %) CNC-APTES was chosen for film preparation. All films were shear cast at 15 s^{-1} onto a polyester film using a Gardco doctor blade film coater (Figure S8). To retain the same amount of CNC in the dried film, the films' wet thickness was 1524 and 3050 μm for CNC and CNC-APTES, respectively. All films were dried at 40 °C for an hour to accelerate gelation and reduce CNC rotational relaxation prior to vitrification. The films were further dried overnight at 25 °C.

Cross-polarized optical microscopy and optical contrast measurements were used to compare the degree of nanocrystal alignment in the dried films. Using a previously published method,[35] optical contrast (OC) was determined based on the overall intensity of representative images (4908 × 3264 pixels, 20× magnification, minimum 15 spots) using

$$OC = \frac{(I_{max} - I_{min})}{(I_{max} + I_{min})} \times 100$$
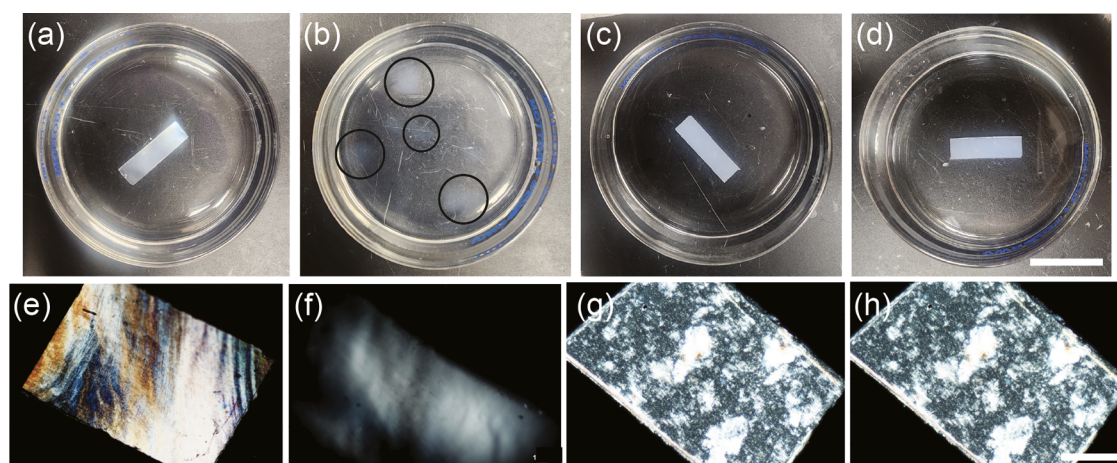
Figure 3. Structural stability of CNC and CNC-APTES films in water; CNC film in water at (a) $t = 0$ h and (b) $t = 2$ h; CNC-APTES film in water at (c) $t = 0$ h and (d) $t > 36$ h. Scale bar represents 20 mm for panels (a−d). Microscopic observation of structural integrity; CNC film in water at (e) $t = 0$ min and (f) $t = 15$ min; CNC-APTES film in water at (g) $t = 0$ min and (h) $t = 15$ min. Scale bar represents 50 μm for panels (e−h).
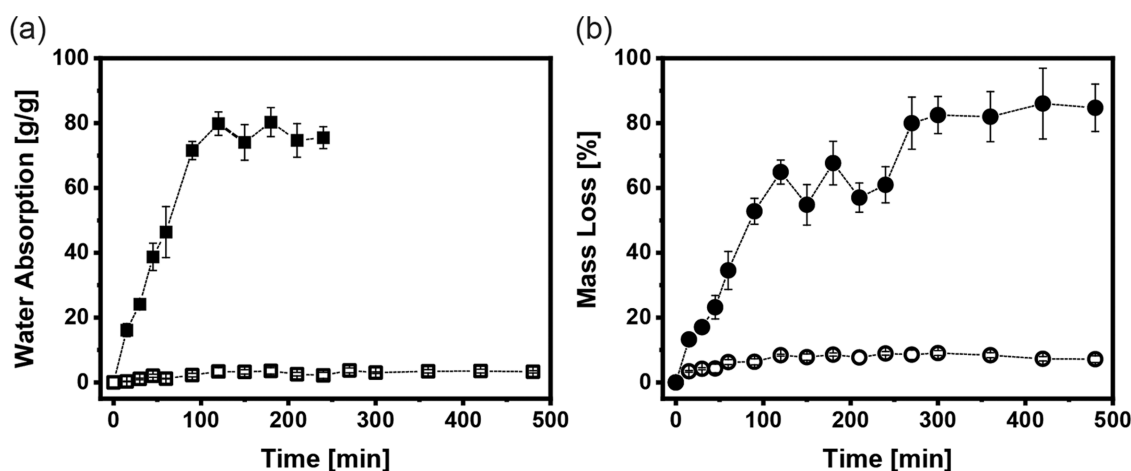
Figure 4. Hydrolytic stability of CNC and CNC-APTES films; (a) time-dependent change in water uptake of 10 mm × 10 mm films placed in strainers (■ CNCs, □ CNC-APTES); (b) time-dependent change in mass loss of 10 mm × 10 mm films placed in strainers (● CNCs, ○ CNC-APTES). The error bar is based on the standard error ($n = 3$). Error bars are smaller than the data points for CNC-APTES.

where I_{max} and I_{min} are the film intensity with polarizer 45 and 0°, respectively, relative to the flow direction. An OC value of 100% indicates complete ordering, whereas negative or 0% OC denotes no significant alignment in the flow direction.[35] Representative cross-polarized optical microscopy images of shear cast CNCs and CNC-APTES films are shown in Figure 2. These images correspond to OC = 30.5 ± 2.8% for the CNC films and OC = 5.5 ± 0.9% for the CNC-APTES films. The higher value for the CNC films is attributed to the presence of significant alignment in the liquid crystalline CNC dispersions compared to the isotropic CNC-APTES dispersions; even drop-cast liquid crystalline CNC dispersions exhibit ordering.[37] The aggregation resulting from APTES cross-linking and lack of liquid crystallinity due to the modification also impacted the alignment in the CNC-APTES film.

2.3. Impact of APTES Modification on Hydrolytic Stability of Shear Cast Films. APTES functionalization had a profound impact on the CNC films' contact angle and hydrolytic stability. The contact angles of the pristine CNC films were 70° ± 7° and 93° ± 4° for the CNC-APTES films. Figure 3a,b shows that the CNC films immersed in water disintegrated to form cloudy, hazy, gelatinous regions 2 h after immersion into the water; after 5 h, even these regions had

dispersed. Although APTES' polar amine group is hydrophilic, silylation of the CNC hydroxyl groups resulted in the CNC-APTES films having significantly greater hydrolytic stability. Even after 3 days, the CNC-APTES films retained their shape. It is noted that after several hours, they did become softer and were challenging to remove from the bath without breaking due to the surface tension of the water. Cross-polarized optical microscopy was used to gain more insight into the temporal changes in the films' structures. Figure 3e,f shows that the CNC films lost some of their birefringence and changed in shape after a mere 15 min. After 20 min, this progressed to them becoming completely isotropic. In contrast, Figure 3g,h shows that the CNC-APTES films did not undergo any noticeable changes in 15 min.

To better quantify the films' water uptake and disintegration, hydrolytic stability tests were performed for different time intervals (see Section 4). The water absorption of each type of film was measured over 4 h by removing samples and measuring their mass before and after drying. As shown in Figure 4a, the CNC films' water absorption increased with time until a plateau of approximately 72 g water/g solid was obtained after 2 h; by this point, the films had transformed into a gel constrained in the strainer. After 4 h, no further data was

reported as the residual material would flow out of the strainer upon removal from the bath. With APTES modification, the water uptake was limited to 3.7 g of water/g of solid mass even after 4 h, and the films retained their rectangular shape. Film disintegration (loss of CNC to the water bath) was quantified based on the mass of dried material remaining in the strainer relative to the initial film mass (Figure 4b). Consistent with visual observation, the CNC films lost more than half their mass in less than 2 h. The remaining gelatinous material continued to lose CNC, resulting in approximately 80% of the mass being lost within 4 h. In contrast, the CNC-APTES mass loss showed an initial increase and then remained steady at less than 10% throughout the 4 h test.

2.4. Impact of APTES Modification on Mechanical Properties of Shear Cast Films.
Mechanical properties of shear cast CNC and CNC-APTES films were evaluated by using tensile testing. Figure 5 shows that APTES modification
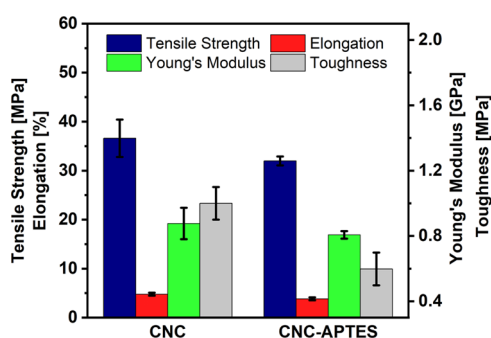
Figure 5. Comparison of mechanical properties: tensile strength, elongation, Young's modulus, and toughness of sheared (15 s^{-1}) CNC and CNC-APTES films. Error bars represent the standard error ($n = 7$).

did not significantly affect most of the films' mechanical properties; this was confirmed using two-sample t-tests with unequal variance. There was no statistically significant difference between the measured average tensile strengths of the CNC and CNC-APTES films (36.6 ± 3.8 and 31.9 ± 0.9 MPa, respectively). The average Young's moduli were nearly identical (0.9 ± 0.1 and 0.8 ± 0.0 GPa for CNC and CNC-APTES films, respectively); these values were calculated from the initial linear region of the stress−strain plots (Figure S9). The CNC films had a slightly higher average elongation at break than the CNC-APTES films (4.8 ± 0.3 and 3.8 ± 0.3%, respectively, $p = 0.054$). The subtle differences in individual property values resulted in statistically significant differences in the films' toughness. The toughness of the CNC films was 1.0 ± 0.1 MPa compared to 0.6 ± 0.1 MPa for CNC-APTES films ($p = 0.044$). While the presence of APTES on the CNCs' surfaces provides some flexibility for dissipating stress, both APTES' disruption of CNC−CNC interactions and CNC-APTES aggregation could account for the decrease in toughness. Since only one shear rate was studied, it is not possible to deconvolute the effects of alignment, as measured by optical contrast, from the effects of chemical modification. However, any changes in properties resulting from differences in alignment would likely be limited to Young's modulus. A previous study by Reising et al.[36] reported increasing Young's modulus with the degree of alignment (order parameter), but statistically significant changes were not observed for tensile strength or the maximum elongation. Similarly, using both

simulations and experiments, Shishebor et al. found that CNC films' Young's moduli increased with Herman's orientation factor in the axial direction parallel to alignment.[38] Their simulations showed orientation had a weak effect on tensile strength, but this was not confirmed experimentally. They found that the most significant changes in simulated properties could be achieved by increasing CNC−CNC interactions.[38] but also highlighted that experimental results are affected by multiple factors including the substrate, drying technique, and initial dispersion concentration.

The mechanical properties of CNC films could not be investigated even after brief water immersion due to their rapid mass loss and lack of mechanical integrity during removal from the water bath. The mechanical properties of CNC-APTES films were determined after short (5 min, denoted as CA5) and long (120 min, denoted as CA120) periods of immersion in water, followed by ambient temperature drying. The 5 and 120 min durations were chosen based on the times for nonspecific sensing and saturation in the sensing studies described in Section 2.5. As shown in Table 2, the tensile strengths and

Table 2. Mechanical Properties of CNC-APTES Films Before and After Water Immersion[a]

property	CNC-APTES	CA5	CA120
tensile strength (MPa)	31.9 (0.9)	41.2 (3.3)	30.2 (2.2)
Young's modulus (GPa)	0.8 (0.0)	0.9 (0.0)	0.8 (0.0)

[a]Number in the parentheses represents the standard error ($n = 7$).

Young's moduli of the initial CNC-APTES and CA120 films were identical ($p > 0.05$). Surprisingly, the CA5 films had greater tensile strengths and Young's moduli than the CNC-APTES and CA120 films. While mechanical properties, are considered bulk properties, the impact of water immersion can have an impact on microscale interactions. The 120 min immersion was likely sufficient time for water diffusion throughout the thickness of the film, resulting in a consistent impact of wetting and drying throughout the films' cross sections. In contrast, 5 min of immersion might have only affected the films' surfaces and resulted in something akin to vitrification layers at the top and bottom surfaces. Redrying these layers may have caused film hardening at surfaces, which impacted the overall tensile and Young's moduli of the films. In addition, a few of the CA5 (43%) and CA120 (57%) films exhibited ductile behavior consisting of necking without fracture (Figure S9). These films were not included in the reported elongation and toughness data. The cause of this behavior and its inconsistency is unknown. However, one possibility is that hydrolysis of APTES converted some Si−O−C to Si−OH.[21] This could enhance hydrogen bonding between both APTES−APTES and CNC-APTES and lead to greater elongation of the films[39] due to the sliding of CNCs in the hydrogen bonding plane[40] that can exist between two APTES groups as well as between APTES and CNCs. The mass loss and resulting free volume within the films may also have been contributed to them becoming more ductile.

2.5. Impact of APTES Modification on the Molecular Interaction with Carbofuran.
Carbofuran, like many other carbamates used in agriculture, can be swept away by rainwater and enter the water cycle. Carbofuran's potential health effects, weak degradability under environmental conditions, and high solubility in water make it an emerging contaminant of concern.[41] Two different techniques, quartz crystal micro-
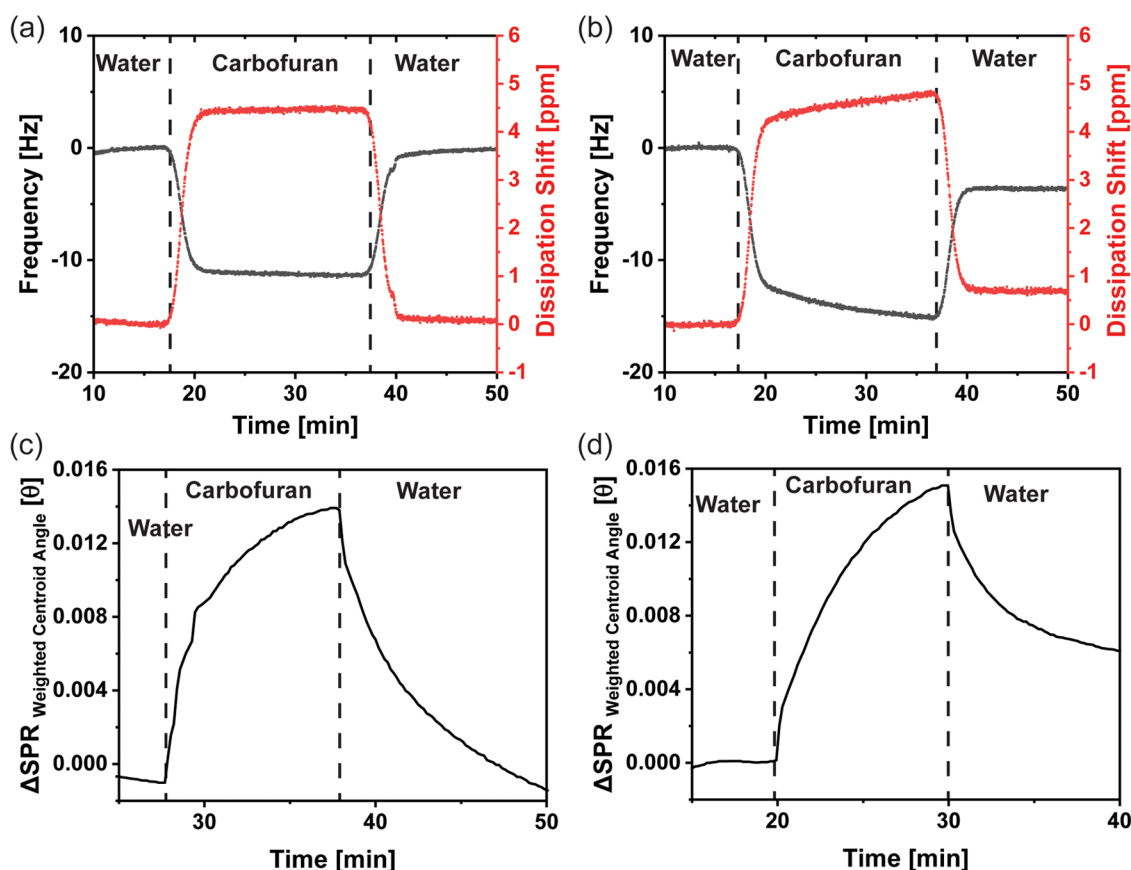
Figure 6. Representative QCMD and MP-SPR sensorgrams of CNC- and CNC-APTES-coated Au sensors; (a) QCMD: interaction of carbofuran (100 ppm) with the CNC film; (b) QCMD: interaction of carbofuran (100 ppm) with the CNC-APTES film (symbol key: black frequency, red dissipation); (c) SPR: interaction of carbofuran (100 ppm) with the CNC film; (d) MP-SPR: interaction of carbofuran (100 ppm) with the CNC-APTES film (channel 1, 670 nm laser). Sensorgrams of additional QCMD and MP-SPR runs are shown in Figures S10 and S11.

balance with dissipation (QCMD) and multiparametric surface plasmon resonance (MP-SPR), were employed to study the interaction of carbofuran with spin-coated CNC and CNC-APTES films, as shown in Figure 6. QCMD is a surface technique that simultaneously monitors the adsorption of the molecules based on frequency shift Δf and energy loss via dissipation shift ΔD. MP-SPR is an optical technique that detects the shift in reflective angle θ due to the change in plasmonic properties. For MP-SPR, two different channels were studied to ensure repeatability, whereas each channel was excited with two different wavelength lasers to excite the plasmons at different levels. Additional MP-SPR sensorgrams are included in Figure S10.

For both methods, ultrapure water was flowed over the CNC- or CNC-APTES-coated sensor until a flat response was observed, indicating the stability of the surface water interactions. This step was defined as Zone 1. After that, 100 ppm aqueous carbofuran solution was introduced and flowed until a stable response was achieved, which resulted in a drop in frequency for QCMD and a positive shift of reflective angle for MP-SPR (Zone 2). Then, in Zone 3, the sensors were flushed with water again to remove loosely bonded carbofuran from the film. The response shift between Zones 2 and 1 shows the reversible attachment of carbofuran, whereas the response shift between Zones 3 and 1 indicates the irreversible attachment of carbofuran. The calculated shifts are provided in Table 3.

Table 3. Nonspecific Molecular Interaction of Carbofuran with CNC and CNC-APTES Films

parameters	CNC film	CNC-APTES film
reversible frequency shift, Δf_{rev} [Hz]	−11.4	−15.3
irreversible frequency shift, Δf_{irr} [Hz]	−0.1	−3.7
reversible dissipation shift, ΔD_{rev} [ppm]	4.8	4.7
irreversible dissipation shift, ΔD_{irr} [ppm]	−0.2	−0.7
reversible angle shift, $\Delta\theta_{rev}$, $\times 10^{-3}$ [°]	15.0	15.0
irreversible angle shift, $\Delta\theta_{irr}$, $\times 10^{-3}$ [°]	0.3	6.1

In terms of reversible binding, QCMD showed a higher Δf for CNC-APTES compared to CNC, although no significant difference in $\Delta\theta$ was observed in the MP-SPR measurements. It should be noted that MP-SPR is an optical technique with inherent limitations concerning film thickness. In addition, the shifts in $\Delta\theta$ were different for different lasers (Figures 6c,d and S10), which can be attributed to the constant values of each laser ($k*d_p = 1 \times 10^{-7}$ nm/degree for 670 nm and 1.9×10^{-7} nm/degree for 785 nm). In Zone 3, the removal of unbound carbofuran resulted in an increase in f and a decrease in θ; the differences in these values from those in Zone 1 indicate irreversible adsorption. Neither QCMD nor MP-SPR showed appreciable irreversible attachment of carbofuran to CNC. However, both methods showed irreversible attachment to CNC-APTES with $\Delta f = -3.7$ Hz and $\Delta\theta = 3 \times 10^{-3°}$, respectively. Changes in dissipation ΔD measured during QCMD provide additional information about the formation of

adsorbed layer formation. Increased dissipation during the flow of carbofuran indicates softer layer formation, but dissipation decreased during the flushing with water in Zone 3. The irreversible shift in dissipation with CNC-APTES was significantly higher compared to CNC films, consistent with the change in film properties resulting from the adsorption of carbofuran molecules. The higher affinity of CNC-APTES to carbofuran molecules can be explained in terms of the availability of the end amine groups, which is more favorable than other possible molecular APTES orientations on the modified CNC.[25] We attribute the increased irreversible adsorption of carbofuran to the electronegative oxygen-containing sites of carbofuran interacting with the positive amine end of CNC-APTES being a stronger interaction than that with the hydroxyl groups readily available on pristine CNCs. It should be noted that the interactions of carbofuran are highly governed by the rotational orientation of nanocrystals, which dictates the exposed functional group at the outer surface. For the spin-coated sensors orientation is a function of substrate, rotation speed, time, and dispersion concentration.[42,43]

3. CONCLUSIONS

While the ability of CNC films to sense humidity via changes in optical properties is well established, their low hydrolytic stability has limited their use as sensors or adsorbents requiring water immersion. Our previous work[30] showed that APTES modification of CNCs could be used as an intermediate for producing biosensors based on antibody−antigen binding. The current study extended our previous work by quantifying the properties of CNC-APTES films. Dry CNC-APTES films exhibited less birefringence and shear alignment than the CNC films but had similar mechanical properties. Notably, CNC-APTES films had considerably greater hydrolytic stability than CNC films. While CNC films immersed in water exhibited significant deterioration in less than 15 min, CNC-APTES films underwent initial moisture adsorption but then retained their shape even after 3 days. This extends the CNC's range of potential applications to those requiring water immersion for hours or days. Compared to CNC films, CNC-APTES films also had greater adsorption of carbofuran, a model pesticide. This result highlights the potential for CNC-APTES chemistry to create useful materials that can be used as adsorbents or sensors without additional modification. Together the results of this research provide a promising foundation for future work on evaluating the stability and adsorption properties of different forms of CNC-APTES, such as films and cryogels, under different environmental conditions and during exposure to a mixture of emerging contaminants.

4. MATERIALS AND METHODS

4.1. Materials. An aqueous sulfated cellulose nanocrystal (CNC) dispersion (6.4 wt %/4.1 vol %, CelluForce NCC Dispersion NCV-100 Prod. #C1A20026) with a Na^+ counterion was obtained from Celluforce, Montreal, Canada. Ethanol (200 proof, ACS grade), 3-aminopropyl-triethoxysilane (APTES, $C_9H_{23}NO_3Si$, 99%), and carbofuran (CF, $C_{12}H_{15}NO_3$, 98%) were purchased from Sigma-Aldrich and used as received. Glacial acetic acid (ACS grade) was obtained from VWR International. Densities of 1.6 g/cm^3 for CNCs and CNC-APTES and 1.0 g/cm^3 for water were used in conversions between concentrations by mass and volume.

Details of the characterization methods for the as-received CNC and modified CNC-APTES are in the Supporting Information (pages S1−S7 and Figures S1−S5)

4.2. CNC-APTES Synthesis. Based on a previously developed method,[30,34] the as-received CNC dispersion was added in an APTES plus solvent (water−ethanol, 80:20 v/v) mixture at a mass ratio of 1.8:1 after adjusting the pH to 4.0 with the addition of glacial acetic acid. It is noted that running the reaction with a higher APTES ratio increased aggregation, most likely due to APTES cross-linking the CNCs. The mixture was tip sonicated for 3 min (90 kJ/g, 750W, 30% amplitude) and then magnetically stirred for 2 h. Two centrifugation washes (2200g, 60 min) were conducted to separate the unreacted APTES and solvent. The resulting CNC-APTES sediment varied from 2.0 to 2.2 vol% (3.2 to 3.5 wt %).

4.3. Dispersion and Film Preparation. The concentration of the as-received CNC dispersion was determined using TGA in argon with a 10 °C/min ramp to 120 °C, followed by an isothermal hold for 45 min. The initial dispersion was then diluted to the desired concentration with ultrapure water (purified using Labconco Water Pro BT, resistivity 18.2 MΩ cm at 25 °C, pH 6.4). The mixture was vortexed for 2 min, followed by overnight bottle rolling. The CNC-APTES dispersion was prepared similarly to obtain the desired concentration. The dispersions were allowed to rest for a minimum of 30 min to avoid bubbles in the cast films. The shear cast films were prepared on a polyester substrate (0.005 in. thick, Grainger) using a Gradco film applicator and MSK-AFA-II automatic film coater (MTI Corporation). The speed was varied based on the wet thickness to achieve a 15 s^{-1} shear rate. The wet films were dried at 40 °C for 1 h (Isotemp Vacuum oven, Fisher Scientific, Model 285A) and then overnight at room temperature (25 °C).

4.4. Hydrolytic Stability. The hydrolytic stability of CNC and CNC-APTES films was evaluated based on the water absorption and mass loss determination. The films were cut into 10 mm × 10 mm pieces and placed inside a nylon cell strainer with a 40-μm pore size (VWR international, #76327−098). The strainers were necessary because the CNC films quickly lost mechanical integrity. The masses of films and strainers that had been stored under ambient conditions were recorded (Figure S12). The films containing strainers were dipped into water at different time intervals. The wet mass was recorded after taking the strainer out of the water. The masses of empty strainers that were soaked in water were also recorded to account for moisture on the strainer itself; this value was subtracted from the total wet mass. Again, due to mechanical integrity issues, it was not possible to blot the films to remove free water; therefore, the measured values include the mass of water sitting on the surface but not actually physisorbed. The final mass was noted after drying the wet films overnight at 100 °C. Then, the following equations were used to calculate the water absorption and mass loss of the films.

$$\text{water absorption}$$
$$= \frac{\text{wet mass} - \text{final dry mass} - \text{water adsorbed on strainer}}{\text{final dry mass}}$$

(2)

$$\text{mass loss} = \frac{\text{initial film mass} - \text{final dry mass}}{\text{initial film mass}} \quad (3)$$

4.5. Mechanical Testing. For tensile testing, the shear cast CNC and CNC-APTES films were cut into 30 mm × 5 mm rectangles, with the long axis parallel to the flow direction.[44] The film strips were cut from the center of the dried film to avoid edge effects. The thickness was measured using an electronic digital micrometer (Marathon part no. CO 030025, resolution 2 μm) at 5 different points for each to calculate the average thickness. The films were glued into 30 mm × 30 mm paper frames with a border thickness of 5 mm, which resulted in a gauge length of 20 mm for the films (Figure S13a). The frame borders were carefully cut on each side before testing. An Instron 5565 was used to conduct tensile testing using a crosshead speed of 0.5 mm/min and a 100N load cell, as shown in Figure S13b,c. Average mechanical property measurements were determined on at least seven films, and a two-sample t-test using unequal variance was used to determine whether the difference between CNC and CNC-APTES films was statistically significant.

4.6. QCMD and MP-SPR Experimentation. Gold QSensors (QSX301) for QCMD and Gold sensor slides (50 nm Au, 2 nm Cr) for MP-SPR were purchased from Nanoscience Instruments and BioNavis, respectively. All of the sensors were washed thoroughly with ethanol and water, followed by 30 min of ozone treatment in the Novascan PSD series Digital UC Ozone System (Iowa). In case of reuse, the sensors were initially cleaned in a solution of NH_4OH, H_2O, and H_2O_2 (at a ratio of 5:1:1, w/w) at 60 °C for 15 min. Sensors were dipped into ultrapure water for 15 min and then cleaned in piranha solution (at a ratio of 3:1 w/w H_2SO_4 and H_2O_2, respectively) for 1 min, followed by a rinse with ultrapure water. The cleaned sensors were coated by immersing in a 0.1 wt % polyethyleneimine solution to create an anchoring layer and then spin-coated with 0.1 wt % CNC or CNC-APTES dispersion at 3000 rpm for 1 min using a VTC-110PA tabletop spin coater and dried at 40 °C overnight. A QSense Analyzer from Biolin Scientific (Västra Frölunda, Sweden) was used to follow changes in frequency and dissipation due to molecular interactions between the coated film and carbofuran. A similar study was conducted using an MP-SPR Navi 210A VASA (BioNavis Ltd., Tampere, Finland) to measure changes in the reflection angle due to the changes in the refractive index resulting from adsorption. Experiments were performed with a constant flow rate of 50 μL/min for QCMD and 20 μL/min for MP-SPR at 25 °C. The same flow rate was maintained for water and the 100 ppm carbofuran solution.

ASSOCIATED CONTENT

Supporting Information

The Supporting Information is available free of charge at https://pubs.acs.org/doi/10.1021/acsomega.4c00439.

> CNC and CNC-APTES characterization (Figures S1−S4); DLS size distribution (Figure S5); CNC-APTES aggregation (Figure S6); CNC dispersion phase images (Figure S7); film coater and stress−strain plot (Figures S8 and S9); additional MP-SPR and QCMD sensorgrams (Figures S10 and S11); hydrolytic stability testing (Figure S12); and tensile testing using Instron 5565 (Figure S13) (PDF)

AUTHOR INFORMATION

Corresponding Author

Virginia A. Davis − *Department of Chemical Engineering, Auburn University, Auburn, Alabama 36849, United States;* orcid.org/0000-0003-3126-3893; Email: davisva@auburn.edu

Authors

Sadat Kamal Amit − *Department of Chemical Engineering, Auburn University, Auburn, Alabama 36849, United States;* orcid.org/0000-0001-7057-0971

Diego Gomez-Maldonado − *Sustainable Biomaterials Lab, College of Forestry, Wildlife, and the Environment, Auburn University, Auburn, Alabama 36849, United States;* orcid.org/0000-0003-4199-4091

Tiana Bish − *Department of Chemical Engineering, Auburn University, Auburn, Alabama 36849, United States*

Maria S. Peresin − *Sustainable Biomaterials Lab, College of Forestry, Wildlife, and the Environment, Auburn University, Auburn, Alabama 36849, United States*

Complete contact information is available at:
https://pubs.acs.org/10.1021/acsomega.4c00439

Author Contributions

The manuscript was written through contributions of all authors. All authors have given approval to the final version of the manuscript.

Notes

The authors declare no competing financial interest.

ACKNOWLEDGMENTS

REFERENCES

(1) Xie, S.; Zhang, X.; Walcott, M. P.; Lin, H. Applications of cellulose nanocrystals: A review. *Eng. Sci.* **2018**, *2*, 4−16.

(2) Moud, A. A. Chiral liquid crystalline properties of cellulose nanocrystals: Fundamentals and applications. *ACS Omega* **2022**, *7* (35), 30673−30699.

(3) Salam, A.; Lucia, L. A.; Jameel, H. A novel cellulose nanocrystals-based approach to improve the mechanical properties of recycled paper. *ACS Sustainable Chem. Eng.* **2013**, *1* (12), 1584−1592.

(4) Wu, X.; Lu, C.; Zhou, Z.; Yuan, G.; Xiong, R.; Zhang, X. Green synthesis and formation mechanism of cellulose nanocrystal-supported gold nanoparticles with enhanced catalytic performance. *Environ. Sci. Nano* **2014**, *1* (1), 71−79.

(5) Jackson, J. K.; Letchford, K.; Wasserman, B. Z.; Ye, L.; Hamad, W. Y.; Burt, H. M. The use of nanocrystalline cellulose for the binding and controlled release of drugs. *Int. J. Nanomed.* **2011**, *6*, 321−330.

(6) Nicharat, A.; Shirole, A.; Foster, E. J.; Weder, C. Thermally activated shape memory behavior of melt-mixed polyurethane/cellulose nanocrystal composites. *J. Appl. Polym. Sci.* **2017**, *134* (27), No. 45033.

(7) Trache, D.; Hussin, M. H.; Haafiz, M. K. M.; Thakur, V. K. Recent progress in cellulose nanocrystals: sources and production. *Nanoscale* **2017**, *9* (5), 1763−1786.

(8) Habibi, Y.; Lucia, L. A.; Rojas, O. J. Cellulose nanocrystals: Chemistry, self-Assembly, and applications. *Chem. Rev.* **2010**, *110* (6), 3479−3500.

(9) Shojaeiarani, J.; Bajwa, D. S.; Hartman, K. Esterified cellulose nanocrystals as reinforcement in poly(lactic acid) nanocomposites. *Cellulose* **2019**, *26* (4), 2349−2362.

(10) Hu, Z.; Berry, R. M.; Pelton, R.; Cranston, E. D. One-pot water-based hydrophobic surface modification of cellulose nanocrystals using plant polyphenols. *ACS Sustainable Chem. Eng.* **2017**, *5* (6), 5018−5026.

(11) Li, Z.; Jiang, X.; Yao, Z.; Chen, F.; Zhu, L.; Liu, H.; Ming, L. Chitosan functionalized cellulose nanocrystals for stabilizing pickering emulsion: Fabrication, characterization and stability evaluation. *Colloids Surf., A* **2022**, *632*, No. 127769.

(12) Abitbol, T.; Marway, H.; Cranston, E. D. Surface modification of cellulose nanocrystals with cetyltrimethylammonium bromide. *Nord. Pulp Pap. Res. J.* **2014**, *29* (1), 46−57.

(13) de Oliveira Taipina, M.; Ferrarezi, M. M. F.; Yoshida, I. V. P.; do Carmo Gonçalves, M. Surface modification of cotton nanocrystals with a silane agent. *Cellulose* **2013**, *20* (1), 217−226.

(14) Shang, W.; Huang, J.; Luo, H.; Chang, P. R.; Feng, J.; Xie, G. Hydrophobic modification of cellulose nanocrystal via covalently grafting of castor oil. *Cellulose* **2013**, *20* (1), 179−190.

(15) Abraham, E.; Nevo, Y.; Slattegard, R.; Attias, N.; Sharon, S.; Lapidot, S.; Shoseyov, O. Highly hydrophobic thermally stable liquid crystalline cellulosic nanomaterials. *ACS Sustainable Chem. Eng.* **2016**, *4* (3), 1338−1346.

(16) Hanif, Z.; Choi, D.; Tariq, M. Z.; La, M.; Park, S. J. Water-stable flexible nanocellulose chiral nematic films through acid vapor cross-linked glutaraldehyde for chiral nematic templating. *ACS Macro Lett.* **2020**, *9* (2), 146−151.

(17) Zhang, F.; Ge, W.; Wang, C.; Zheng, X.; Wang, D.; Zhang, X.; Wang, X.; Xue, X.; Qing, G. Highly strong and solvent-resistant cellulose nanocrystal photonic films for optical coatings. *ACS Appl. Mater. Interfaces* **2021**, *13* (14), 17118−17128.

(18) Yu, H.-Y.; Chen, R.; Chen, G.-Y.; Liu, L.; Yang, X.-G.; Yao, J.-M. Silylation of cellulose nanocrystals and their reinforcement of commercial silicone rubber. *J. Nanopart. Res.* **2015**, *17* (9), 361.

(19) Ludovici, F.; Hartmann, R.; Rudolph, M.; Liimatainen, H. Thiol-silylated cellulose nanocrystals as selective biodepressants in froth flotation. *ACS Sustainable Chem. Eng.* **2023**, *11* (45), 16176−16184.

(20) Kim, H.; Youn, J. R.; Song, Y. S. Eco-friendly flame retardant nanocrystalline cellulose prepared via silylation. *Nanotechnology* **2018**, *29* (45), No. 455702.

(21) Ludovici, F.; Hartmann, R.; Liimatainen, H. Aqueous bifunctionalization of cellulose nanocrystals through amino and alkyl silylation: functionalization, characterization, and performance of nanocrystals in quartz microflotation. *Cellulose* **2023**, *30* (2), 775−787.

(22) Kaur, A.; Kapoor, S.; Bharti, A.; Rana, S.; Chaudhary, G. R.; Prabhakar, N. Gold-platinum bimetallic nanoparticles coated 3-(aminopropyl)triethoxysilane (APTES) based electrochemical immunosensor for vitamin D estimation. *J. Electroanal. Chem.* **2020**, *873*, No. 114400.

(23) Can, K.; Ozmen, M.; Ersoz, M. Immobilization of albumin on aminosilane modified superparamagnetic magnetite nanoparticles and its characterization. *Colloids Surf., B* **2009**, *71* (1), 154−159.

(24) Qiao, B.; Wang, T.-J.; Gao, H.; Jin, Y. High density silanization of nano-silica particles using γ-aminopropyltriethoxysilane (APTES). *Appl. Surf. Sci.* **2015**, *351*, 646−654.

(25) Acres, R. G.; Ellis, A. V.; Alvino, J.; Lenahan, C. E.; Khodakov, D. A.; Metha, G. F.; Andersson, G. G. Molecular structure of 3-aminopropyltriethoxysilane layers formed on silanol-terminated silicon surfaces. *J. Phys. Chem. C* **2012**, *116* (10), 6289−6297.

(26) Khanjanzadeh, H.; Behrooz, R.; Bahramifar, N.; Gindl-Altmutter, W.; Bacher, M.; Edler, M.; Griesser, T. Surface chemical functionalization of cellulose nanocrystals by 3-aminopropyltriethoxysilane. *Int. J. Biol. Macromol.* **2018**, *106*, 1288−1296.

(27) Karami, K.; Saadatzadeh, H.; Ramezanpour, A. Synthesis and characterization of palladium nanoparticles immobilized on modified cellulose nanocrystals as heterogeneous catalyst for reduction of nitroaromatic compounds. *ChemistrySelect* **2021**, *6* (11), 2746−2759.

(28) Reale Batista, M. D.; Drzal, L. T. Carbon fiber/epoxy matrix composite interphases modified with cellulose nanocrystals. *Compos. Sci. Technol.* **2018**, *164*, 274−281.

(29) Rafieian, F.; Jonoobi, M.; Yu, Q. A novel nanocomposite membrane containing modified cellulose nanocrystals for copper ion removal and dye adsorption from water. *Cellulose* **2019**, *26* (5), 3359−3373.

(30) Nori, U. M.; Gomez-Maldonado, D.; Saha, P.; Ashurst, W. R.; Peresin, M. S.; Davis, V. A. Antibody immobilization on sulfated cellulose nanocrystals. *Biomacromolecules* **2023**, *24* (3), 1103−1110.

(31) Eyley, S.; Thielemans, W. Surface modification of cellulose nanocrystals. *Nanoscale* **2014**, *6* (14), 7764−7779.

(32) Vinzant, K.; Clouse, D. E.; Amit, S. K.; Ivanov, I. N.; Davis, V. A.; Khodakovskaya, M. V. Cellulose nanocrystals are a renewable and biocompatible nanocarrier of agrochemicals directly to plant cells. *Adv. Sustainable Syst.* **2023**, No. 2300511.

(33) Foster, E. J.; Moon, R. J.; Agarwal, U. P.; Bortner, M. J.; Bras, J.; Camarero-Espinosa, S.; Chan, K. J.; Clift, M. J. D.; Cranston, E. D.; Eichhorn, S. J.; et al. Current characterization methods for cellulose nanomaterials. *Chem. Soc. Rev.* **2018**, *47* (8), 2609−2679.

(34) Nori, U. M. Antibody-Immobilized Cellulose Nanocrystals for the Detection of Cancer Biomarkers. M.Sc. thesis, Auburn University: Auburn, AL, 2019.

(35) Haywood, A. D.; Davis, V. A. Effects of liquid crystalline and shear alignment on the optical properties of cellulose nanocrystal films. *Cellulose* **2017**, *24* (2), 705−716.

(36) Reising, A. B.; Moon, R. J.; Youngblood, J. P. Effect of particle alignment on mechanical properties of neat cellulose nanocrystal films. *J. Sci. Technol. For. Prod. Processes* **2012**, *2* (6), 32−41.

(37) Pritchard, C. Q.; Navarro, F.; Roman, M.; Bortner, M. J. Multi-axis alignment of rod-like cellulose nanocrystals in drying droplets. *J. Colloid Interface Sci.* **2021**, *603*, 450−458.

(38) Shishehbor, M.; Son, H.; Nuruddin, M.; Youngblood, J. P.; Davis, C.; Zavattieri, P. D. Influence of alignment and microstructure features on the mechanical properties and failure mechanisms of cellulose nanocrystals (CNC) films. *J. Mech. Behav. Biomed. Mater.* **2021**, *118*, No. 104399.

(39) Wei, X.-Y.; Lin, T.; Wang, L.; Yin, X.-F. Effect of a limited amount of d-sorbitol on pitch and mechanical properties of cellulose nanocrystal films. *Crystals* **2021**, *11*, No. 1324.

(40) Csiszár, E.; Nagy, S. A comparative study on cellulose nanocrystals extracted from bleached cotton and flax and used for casting films with glycerol and sorbitol plasticisers. *Carbohydr. Polym.* **2017**, *174*, 740−749.

(41) Richardson, S. D.; Ternes, T. A. Water analysis: Emerging contaminants and current Issues. *Anal. Chem.* **2018**, *90* (1), 398−428.

(42) Jiang, M.; DeMass, S.-N.; Economy, D.-R.; Shackleton, T.; Kitchens, C.-L. Formation of highly oriented cellulose nanocrystal films by spin coating film from aqueous suspensions. *J. Renewable Mater.* **2016**, *4* (5), 377−387.

(43) Cranston, E. D.; Gray, D. G. Birefringence in spin-coated films containing cellulose nanocrystals. *Colloids Surf., A* **2008**, *325* (1), 44−51.

(44) Passantino, J. M.; Haywood, A. D.; Goswami, J.; Davis, V. A. Effects of polymer additives and dispersion state on the mechanical properties of cellulose nanocrystal films. *Macromol. Mater. Eng.* **2017**, *302* (4), No. 1600351.